

# 1 Characterization of secondary organic aerosol from heated- 2 cooking oil emissions: evolution in composition and volatility

3 Manpreet Takhar<sup>1</sup>, Yunchun Li<sup>2</sup>, Arthur W. H. Chan<sup>1</sup>

4 <sup>1</sup>Department of Chemical Engineering and Applied Chemistry, University of Toronto, Toronto, M5S 3E5, Canada

5 <sup>2</sup>College of Science, Sichuan Agricultural University, Ya'an, 625014, China

6 *Correspondence to:* Arthur W. H. Chan (arthurwh.chan@utoronto.ca)

7 **Abstract.** Cooking emissions account for a major fraction of urban organic aerosol. It is therefore important to  
8 understand the atmospheric evolution in the physical and chemical properties of organic compounds emitted from  
9 cooking activities. In this work, we investigate the formation of secondary organic aerosol (SOA) from oxidation of  
10 gas-phase organic compounds from heated cooking oil. The chemical composition of cooking SOA is analyzed using  
11 thermal desorption-gas chromatography-mass spectrometry (TD-GC/MS). While the particle-phase composition of  
12 SOA is a highly complex mixture, we adopt a new method to achieve molecular speciation of the SOA. All the GC  
13 elutable material is classified by the constituent functional groups, allowing us to provide a molecular description of  
14 its chemical evolution upon oxidative aging. Our results demonstrate an increase in average oxidation state (from -0.6  
15 to -0.24), and decrease in average carbon number (from 5.2 to 4.9) with increasing photochemical aging of cooking  
16 oil, suggesting that fragmentation reactions are key processes in the oxidative aging of cooking emissions within 2  
17 days equivalent of ambient oxidant exposure. Moreover, we estimate that aldehyde precursors from cooking emissions  
18 account for a majority of the SOA formation and oxidation products. Overall, our results provide insights into the  
19 atmospheric evolution of cooking SOA, a majority of which is derived from gas-phase oxidation of aldehydes.

## 21 1 Introduction

22 Organic aerosol (OA) has important impacts on air quality, climate and human health (Hallquist et al., 2009). OA is  
23 often composed of thousands of organic compounds formed from a variety of sources. In urban areas, particulate  
24 emissions from food cooking account for a significant fraction of OA (Allan et al., 2010; Crippa et al., 2013; Florou  
25 et al., 2017; Kostenidou et al., 2015; Lee et al., 2015; Mohr et al., 2012; Sun et al., 2011). Furthermore, volatile organic  
26 compounds (VOCs) are also emitted, and they can undergo oxidation and form secondary organic aerosol (SOA).  
27 Recent studies have reported the formation of SOA from meat charbroiling (Kaltsonoudis et al., 2017) and heated  
28 cooking oils (Liu et al., 2017b, 2017c, 2018). Therefore, food cooking activities have substantial impacts on air quality  
29 in and downwind of urban areas.

30 The emission of VOCs from cooking is highly variable and depends on a number of factors such as cooking style,  
31 food, ingredients, and temperature (Fullana et al., 2004a, 2004b; Klein et al., 2016a, 2016b; Liu et al., 2017c; Schauer  
32 et al., 1999, 2002). Of the different classes of VOCs characterized in these studies, aldehydes have been shown to be

33 the major group of VOCs emitted from cooking oils. These VOCs are chemically produced upon heating via peroxy  
34 radical reactions of the fatty acids (Choe and Min, 2007; Gardner, 1989). Klein et al. (2016a) investigated the  
35 composition of nonmethane organic gas (NMOG) emissions from boiling, charbroiling, shallow and deep frying of  
36 various vegetables, meats, and cooking oils heated under different temperature conditions. The authors reported that  
37 emissions from shallow frying, deep frying and charbroiling are dominated by aldehydes, and the relative amounts  
38 depend on the type of oil used during cooking (Klein et al., 2016a). C7 aldehydes are the major species in emissions  
39 from canola oil, whereas C9 aldehydes are dominant from olive oil (Klein et al., 2016a). These differences in emission  
40 patterns of oils vary with composition of triglycerides present in the oil (Choe and Min, 2006). Katragadda et al.  
41 (2010) demonstrated up to an order of magnitude increase in emissions upon reaching the smoke point of cooking  
42 oils. In addition to emissions from cooking oil, the addition of condiments (herbs and peppers) to cooking leads to  
43 significant emissions of mono-, sesqui- and diterpenes in the gas phase (Klein et al., 2016b). Liu et al. (2017a) showed  
44 an order of magnitude increase in the emissions of VOCs when stir-frying with spices. Therefore, factors like cooking  
45 style, food, cooking temperature, and ingredients play a significant role in the chemical profile of cooking emissions  
46 (Fullana et al., 2004a, 2004b; Klein et al., 2016a, 2016b; Liu et al., 2017a, 2017c).

47 The VOCs emitted from cooking have been shown to produce significant amount of SOA rapidly in recent flow tube  
48 (Liu et al., 2017b) and smog chamber studies (Kaltsonoudis et al., 2017; Liu et al., 2017c, 2018). Kaltsonoudis et al.  
49 (2017) and Liu et al. (2017b, 2018) showed an increase in O/C ratio upon a few hours of atmospheric aging suggesting  
50 lightly oxidized cooking SOA. Furthermore, Liu et al. (2017b) showed significant production of SOA with increasing  
51 OH exposure for different cooking oils. Thus far studies have only focused on formation potential of SOA from  
52 cooking emissions. Despite high emission rates of VOCs from cooking, the understanding of SOA composition from  
53 these emissions remains limited.

54 Source apportionment using aerosol mass spectrometry (AMS) data in urban areas has often revealed a Cooking  
55 Organic Aerosol (COA) factor, but it is unclear how this factor is related to cooking emissions. Many studies reported  
56 that the mass spectra associated with this factor resemble that of hydrocarbon-like organic aerosol (HOA) factor from  
57 other non-cooking sources (Dall'Osto et al., 2015; Hayes et al., 2013; Huang et al., 2010; Mohr et al., 2009, 2012). In  
58 addition, it is often unclear whether ambient COA represents primary or secondary organic aerosol from cooking  
59 emissions (Dall'Osto et al., 2015; Florou et al., 2017; Kaltsonoudis et al., 2017; Kostenidou et al., 2015). Laboratory  
60 studies (Liu et al., 2017b, 2018) showed that the mass spectra for primary cooking organic aerosol exhibited strong  
61 correlation with ambient COA factor (Lee et al., 2015), but the cooking SOA mass spectra showed some similarities  
62 to ambient semi-volatile oxygenated OA (SV-OOA) factor. These measurements highlight the challenges in assigning  
63 COA factor without understanding the changes in chemical composition occurring during oxidation of cooking  
64 emissions.

65 In general, there is a need to better understand the molecular composition contributing to aged COA. In this study, we  
66 investigate detailed chemical composition of cooking SOA at the molecular level. The objectives of this study are to:  
67 (i) understand the detailed chemical speciation of cooking SOA using TD-GC/MS, (ii) describe chemical evolution in  
68 SOA upon atmospheric aging, and (iii) attribute formation of SOA to different VOCs emitted from food cooking

69 emissions. In this work we use heated cooking oil as a model for food cooking emissions. We show that the majority  
70 of the SOA is derived from oxidation of aldehydes, and the oxidation mechanisms are dominated by fragmentation  
71 reactions. Overall, our results provide useful insights into the evolution of cooking SOA, which may be incorporated  
72 into chemical transport models for better predicting OA formation from cooking emissions in the atmosphere.

73

## 74 **2 Experimental methods**

### 75 **2.1 Flow tube experiments**

76 The experimental setup is shown in Fig. 1, and experimental conditions are listed in Table S1. For each experiment,  
77 30-40 mL of canola oil was heated at 250 °C on an electric heating plate in a Pyrex bottle resulting in an average  
78 cooking oil temperature of 180 °C, as measured by a thermocouple in direct contact with the heated oil. Purified air  
79 flowed over the headspace of the heated oil at a rate of 0.2 L min<sup>-1</sup> and then diluted by a factor of 50. 0.2 L min<sup>-1</sup> of  
80 the total diluted flow was passed through a Teflon filter to remove particles, and the oil vapors were introduced into a  
81 custom-built 10 L quartz flow tube reactor. A separate flow of oxygen (99.6%) was irradiated in a UV ozone generator  
82 (UVP 97006601) to produce ozone and was also introduced into the flow tube reactor. In parallel, purified air was  
83 flowed through a water bubbler into the reactor to provide water vapor. The combined flow rate through the flow tube  
84 was set at 3 L min<sup>-1</sup>, resulting in an average residence time of approximately 200 s.

85 In the flow tube, hydroxyl radicals were produced through the photolysis of ozone irradiated by a UV lamp ( $\lambda = 254$   
86 nm) in the presence of water vapor. The integrated OH exposure was measured indirectly from the loss of cyclopentane  
87 which was monitored by a gas chromatography-flame ionization detector (GC-FID, model 8610C, SRI Instruments  
88 Inc.) equipped with a Tenax TA trap sampling downstream of the flow tube at a rate of 0.15 L min<sup>-1</sup>. In this study, the  
89 experiments were conducted at different OH exposures ranging from  $5.77 \times 10^{10}$  to  $2.2 \times 10^{11}$  molecules cm<sup>-3</sup> s. OH  
90 exposure in this range is equivalent to ~11 to 41 h of atmospheric oxidation, respectively, assuming a 24-h average  
91 atmospheric OH concentration of  $1.5 \times 10^6$  molecules cm<sup>-3</sup> (Mao et al., 2009). The effect of ozone on the SOA  
92 formation was found to be negligible as the reaction timescales of aldehydes with ozone were calculated to be at least  
93 100 times longer than those with OH. A sample calculation for methacrolein reaction timescales with OH and ozone  
94 is shown in SI in Sect. 1.

95 Downstream of the flow tube, pre-baked quartz fiber filter and Tenax tube samples were collected for offline chemical  
96 analysis. The changes in the particle size distribution and volume concentration were monitored using a scanning  
97 mobility particle sizer (SMPS) with a differential mobility analyzer (TSI 3081), and a condensation particle counter  
98 (TSI 3781). A constant density of 1.4 g cm<sup>-3</sup> was assumed to convert particle volume concentration into mass  
99 concentration (Chan et al., 2010). Relative humidity and temperature were monitored by an Omega HX94C RH/T  
100 transmitter and were maintained at 65-70%, and 19-20 °C, respectively for all experiments. A fast stepping/scanning  
101 thermodenuder (TD, Aerodyne Inc. Billerica, USA) was also placed downstream of the flow tube to measure SOA  
102 evaporation rates. Details about TD operating conditions and analysis can be found in Takhar et al. (2019). The TD

103 was only operated during one experiment in which the OH exposure was  $9.23 \times 10^{10}$  molecules  $\text{cm}^{-3}$  s. The SOA was  
104 systematically heated in a TD from 25 °C to 175 °C, and changes in particle volume concentrations and corresponding  
105 mass fraction remaining (MFR) were measured using a SMPS. The SOA size distribution during TD operation and  
106 volatility distribution are shown in Fig. S1 and S2, respectively. A kinetic mass transfer model developed by Riipinen  
107 et al. (2010) was used to interpret the TD data. The inputs to the model are volatility distribution of OA, enthalpy of  
108 vaporization, and mass accommodation coefficients. Compound groups are translated into volatility distributions by  
109 binning components according to their saturation concentrations (Donahue et al., 2006). Parameterization for enthalpy  
110 of vaporization was similar to that of Takhar et al. (2019). We assume a surface tension of  $0.05 \text{ N m}^{-1}$ , gas-phase  
111 diffusion coefficients of  $5 \times 10^{-6} \text{ m}^2 \text{ s}^{-1}$  for all simulations similar to that reported in Riipinen et al. (2010).

112

## 113 2.2 Chemical characterization of SOA

114 Tenax tube and quartz filter samples were analyzed separately by thermal desorption gas chromatography mass  
115 spectrometry (TD-GC/MS) for detailed chemical speciation of gas- and particle-phase organic compounds. The  
116 analyses were performed using a thermal desorption system (TDS 3, Gerstel) combined with a gas chromatography  
117 (7890B, Agilent)-mass spectrometer (5977A, Agilent). For gas-phase analysis, concentrations of aldehydes (C7 to  
118 C10 *n*-alkanals, alkenals and alkadienals) collected on Tenax tube samples before photooxidation (downstream of the  
119 flow tube, with lights off) were quantified. For particle-phase analysis, thermal desorption of quartz filters was  
120 performed with *in situ* derivatization using *N*-trimethylsilyl-*N*-methyl trifluoroacetamide (MSTFA). A known amount  
121 of deuterated 3-hydroxy-1,5-pentanedioic-2,2,3,4,4- $\text{d}_5$  acid, and *n*-pentadecane- $\text{d}_{32}$  (CDN isotopes) was injected,  
122 respectively, onto quartz filter punches, and Tenax tubes as internal standards before the samples were desorbed in  
123 the TDS. All GC/MS analysis was performed using a non-polar DB5 column (Rxi-5Sil MS, Restek). Details of the  
124 operating parameters (GC column, GC and TDS temperature ramps, MS parameters) can be found in Sect. 2 of SI.

125 With *in situ* derivatization, polar organic compounds react rapidly with MSTFA at elevated temperatures during  
126 thermal desorption, and functional groups with acidic hydrogen atoms (such as –OH) are replaced by a less polar  
127 trimethylsilyl (TMS, [-OSi(CH<sub>3</sub>)<sub>3</sub>]) group. This reduction in polarity allows the derivatized analyte to elute from a  
128 non-polar column and analyzed by subsequent electron impact (EI) at 70 eV. Derivatized compounds produce a  
129 signature fragment ion at mass-to-charge ( $m/z$ ) 73 (-Si(CH<sub>3</sub>)<sub>3</sub><sup>+</sup>) arising from the scission of O-Si bond in R-O-  
130 [Si(CH<sub>3</sub>)<sub>3</sub>]. In other words, all derivatized compounds produce ions with  $m/z$  73 during analysis. Therefore, the total  
131 signal at  $m/z$  73 can be taken as the total concentration of organic compounds with at least one hydroxyl group  
132 (including both –OH and –C(O)OH) present in cooking SOA, much like how  $m/z$  57 represents total concentration of  
133 aliphatic compounds in hydrocarbon mixtures (Zhao et al., 2014, 2015). It should be noted that organic peroxides (R-  
134 OOH) were also found to be derivatized, but the major reaction product formed is R-O-[Si(CH<sub>3</sub>)<sub>3</sub>] (which is also  
135 formed from R–OH derivatization) as shown in Fig. S3. Here we assume alcohols and acids are the major components,  
136 but will explore the potential role of ROOH on the overall chemical composition in Sect. 3.1.

137 As shown in Fig. 2, many compounds in cooking SOA contain at least one –OH group and the chromatogram of  $m/z$   
 138 73 is typical of that for a highly complex mixture or unresolved complex mixture (UCM). Using traditional analytical  
 139 techniques like GC/MS it is difficult to deconvolute the UCM. However, knowledge about mass spectral  
 140 fragmentation of TMS derivatives can be used to understand the compounds contributing to the UCM. Table S2 shows  
 141 a list of compounds containing multiple functional groups e.g. –COOH, –OH resulting in different combinations of  
 142 compound classes like dicarboxylic acids, hydroxy acids, hydroxy dicarboxylic acids, and dihydroxy dicarboxylic  
 143 acids with different carbon numbers. As mentioned earlier, we acknowledge the potential contribution from ROOH,  
 144 but will first assume the functional groups shown in Table S2 here, and consider ROOH in more detail in a later  
 145 section. The compound groups shown in Table S2 are expected to be formed from oxidation of aldehydes and be  
 146 derivatized by MSTFA. The TMS derivatives of these compounds share common ion fragments in their EI mass  
 147 spectra:  $m/z$  73  $[\text{Si}(\text{CH}_3)_3]^+$ , 75, 147  $[(\text{CH}_3)_2\text{Si}=\text{O}(\text{CH}_3)_3]^+$ , M-15  $[\text{M}-\text{CH}_3]^+$  (Jaoui et al., 2004, 2005; Yu et al., 1998).  
 148 Most importantly, all TMS derivatives exhibit quantifiable peaks at  $m/z$  73 (ubiquitous ion for all derivatives) and M-  
 149 15 (ion specific to each compound group, hereby referred to as the pseudo-parent ion). We also obtained the  
 150 characteristic ratio of these two ions for each compound group ( $f_{M-15/73}$ ) from NIST mass spectral libraries and from  
 151 analyzing authentic standards. To verify the validity of this method, we calculate the total  $m/z$  73 ion signal that is  
 152 attributable to these compound groups by taking the chromatograms of the pseudo-parent ion for each compound  
 153 group, dividing by its characteristic ratio  $f_{M-15/73}$  and then summing across all compound groups as shown in Eq.  
 154 (1).

$$155 \quad S_{73,t}^{sum} = \sum_i \frac{S_{M-15,i,t}}{f_{M-15/73,i}} \quad (1)$$

156 where  $S_{73,t}^{sum}$  is the  $m/z$  73 ion signal at retention time  $t$  that is attributable to all compound groups listed in Table S2,  
 157  $S_{M-15,i,t}$  is the signal of the pseudo-parent ion for compound group  $i$  at retention time  $t$ ,  $f_{M-15/73,i}$  is the characteristic  
 158 ratio of pseudo-parent ion to  $m/z$  73. This approach is similar to that described in Isaacman-VanWertz et al. (2020).  
 159 As shown in Fig. 2,  $S_{73,t}^{sum}$  shows excellent agreement with the measured  $m/z$  73 ion signal, suggesting that the  $m/z$  73  
 160 signal, which is representative of all TMS derivatives, is almost entirely comprised of contributions from the  
 161 compound groups listed in Table S2. This agreement between our bottom-up approach and measured signal provides  
 162 confidence that our method is able to provide information about the chemical composition of highly complex mixture.

163 With the signals from all the pseudo parent ions for all compound groups, the total mass of each compound group was  
 164 then calculated using Eq. (2).

$$165 \quad M_i = \frac{TA_i}{RF_i} \times \frac{1}{f_{M-15/73,i}} \quad (2)$$

166 where,  $M_i$  is the mass of compound group  $i$ ,  $TA_i$  is the total integrated signal of pseudo-parent ion for compound  
 167 group  $i$  (normalized by the signal of deuterated internal standard),  $RF$  is the response factor (calculated from  
 168 calibration curves of fatty acids and dicarboxylic acids authentic standards) of compound group  $i$ , and  $f_{M-15/73,i}$  is  
 169 the characteristic ratio of pseudo-parent ion to  $m/z$  73 for compound group  $i$ . A more detailed, step-by-step description

170 of the procedure can be found in the SI in Sect. 3, and illustrated in Fig. S4 with corresponding uncertainties in the  
171 fitting procedure shown in Fig. S5.

172

### 173 3 Results and discussion

#### 174 3.1 Chemical evolution of SOA

175 As described in Sect. 2.2, components in cooking SOA were classified by functional groups and carbon number. To  
176 describe the overall changes in SOA composition with increasing OH exposure, we use the average carbon oxidation  
177 state ( $\overline{\text{OSc}}$ ) as a metric for the evolving composition of a complex mixture undergoing oxidation (Kroll et al., 2011).  
178 Both  $\overline{\text{OSc}}$  and number of carbon atoms (nc) for each compound group are calculated from the GC-derived chemical  
179 composition. The total mole fraction of C, H and O was calculated for each sample which was then used to calculate  
180 the bulk  $\overline{\text{OSc}}$  using the Eq.  $2 \times O:C - H:C$  (Kroll et al., 2011). The evolution in this framework for canola oil SOA  
181 is shown in Fig. 3. The bulk  $\overline{\text{OSc}}$  was observed to increase from -0.6 to -0.24 when OH exposure increased from 5.77  
182 to  $22.0 \times 10^{10}$  molecules  $\text{cm}^{-3}$  s for canola oil SOA. For comparison, Liu et al. (2017b) showed an initial decrease in  
183  $\overline{\text{OSc}}$  and O:C, but gradually stabilized at OH exposure greater than  $9 \times 10^{10}$  molecules  $\text{cm}^{-3}$  s. For the  $\overline{\text{OSc}}$  range reported  
184 here, the  $\overline{\text{OSc}}$  of cooking SOA falls in the range of SV-OOA as determined from factor analysis of AMS data  
185 (Canagaratna et al., 2015). This degree of oxygenation is greater than that of the COA factor measured by AMS, which  
186 is reported to be around -1.37 (Canagaratna et al., 2015). This difference suggests that the COA factor resolved using  
187 PMF analysis is likely of primary origin and does not represent SOA formed from atmospheric oxidation of cooking  
188 emissions. Furthermore, previous GC/MS analysis showed for POA from cooking oils, an  $\overline{\text{OSc}}$  of -1.66 (canola oil)  
189 and -1.7 (beef tallow, olive oil) was calculated (Takhar et al., 2019). These observations again suggest that COA factor  
190 measured by AMS represents primary cooking emissions.

191 In addition to carbon oxidation state, knowledge about molecular composition provides further insights into the  
192 oxidation mechanisms. Canola oil SOA at an OH exposure of  $5.77 \times 10^{10}$  molecules  $\text{cm}^{-3}$  s is comprised of ~19%  
193 larger (C8-C10) and less oxygenated compounds, this fraction declined to ~11% at higher OH exposures. Furthermore,  
194 the total fraction of C2-C7 products increased from 81% to 89% when OH exposure increased from 10.7 h to 1.7 d.  
195 Of this fraction, the smaller carbon # compounds (C2-C4) which are indicative of fragmentation processes increased  
196 from 42% at 10.7 h to ~49% at 1.7 d. An increase in smaller and more oxygenated compounds, along with decrease  
197 in larger and less oxygenated products suggests that fragmentation reactions are responsible for the shift towards  
198 formation of smaller oxygenated compounds. As a result, oxidation simultaneously leads to higher  $\overline{\text{OSc}}$  and lower  
199 carbon number on average. Based on the compounds observable by our technique, this trend suggests that  
200 fragmentation reactions are key processes in the oxidative evolution of cooking emissions.

201 The compounds observed here can also be compared to previously measured bulk composition using elemental ratios,  
202 such as those presented in a Van Krevelen (VK) diagram (Heald et al., 2010). As shown in Fig. 4, the O:C ratio in our

203 study ranged between 0.64 and 0.79 when OH exposure increased from  $5.77 \times 10^{10}$  to  $22.0 \times 10^{10}$  molecules  $\text{cm}^{-3}$  s. The  
204 O:C ratios measured using an AMS (Kaltsonoudis et al., 2017; Liu et al., 2017b) ranged between 0.24-0.46 which are  
205 within a factor of 2 measured in this study. Furthermore, the H:C versus O:C trend is linear with a slope of -0.19,  
206 which lies between the slope of 0 measured for low- $\text{NO}_x$  oxidation reported by Liu et al. (2017b) and -0.4 for high-  
207  $\text{NO}_x$  conditions (Liu et al., 2018). Therefore, based on elemental ratios, the evolution in SOA composition measured  
208 in this study is comparable to that in bulk average properties estimated by AMS. Furthermore, we use 2D-VBS  
209 framework developed by Donahue et al. (2012) to investigate OA chemistry, and understand the evolution of cooking  
210 SOA through changes in the volatility of SOA system. The vapor pressures of the identified compounds are calculated  
211 using group contribution method (Pankow and Asher, 2008) where experimentally determined vapor pressures were  
212 unavailable, and reported in Table S2. The observed compounds in SOA have a broad range of volatilities, since they  
213 were formed from oxidation of a complex ensemble of VOC precursors. As shown in Fig. S6, there is minor decrease  
214 in overall volatility of the mixture (change lies within one decade in  $C^*$ ) irrespective of the presence of peroxides,  
215 while  $\overline{\text{OSc}}$  is increasing with oxidation. This increase in oxidation state is coincident with increasing fragmentation  
216 upon oxidation, and, as a result, the overall change in the bulk volatility of canola oil SOA is relatively small.

217 As mentioned earlier in Sect. 2.2, there is a potential to misclassify ROOH as ROH using our current GC/MS method.  
218 In Fig. S3, we show that derivatization of cumene hydroperoxide forms the TMS of hydroxy-cumene in our system.  
219 Here we further examine the chemical composition by assuming that each  $-\text{O}[\text{Si}(\text{CH}_3)_3]$  group observed originates  
220 from an  $-\text{OOH}$  group in the SOA. It should be noted that replacing  $-\text{OH}$  with  $-\text{OOH}$  results in a higher estimate of  
221 O:C (and  $\overline{\text{OSc}}$ ) but does not change H:C or carbon #. Furthermore, since pseudo molecular ion fraction ( $f_{M-15/73}$ ) for  
222 organic peroxides (needed for quantification) is unknown, we assume that it is similar to those presented in Table S2.  
223 As shown in Fig. S7, if all observed  $-\text{OH}$  groups are  $-\text{OOH}$  groups, the VK-slope would be -0.15, which is similar to  
224 -0.19 calculated based on the no-peroxide assumption. Similarly, Fig. S6 shows that this uncertainty in hydroxyl group  
225 identification has negligible effect on estimation of vapor pressure or volatility in the 2D-VBS framework. Therefore,  
226 this potential misclassification of peroxide groups may lead to an underestimation in O:C and  $\overline{\text{OSc}}$ , but is not expected  
227 to affect estimates of volatility and our general conclusions about the importance of fragmentation reactions. In the  
228 future, analytical techniques such as extractive electrospray ionization time-of-flight mass spectrometry (Lopez-  
229 Hilfiker et al., 2019) may be useful to better understand the composition of peroxides from cooking SOA. While the  
230 misclassification of peroxides may have little impact on the bulk properties such as average O:C ratios, there may be  
231 important implications on understanding the reactivity of the SOA.

232

### 233 3.2 Evaporation rates of SOA

234 The volatility of the SOA is also probed by measuring the evaporation rates in a heated thermodenuder and compared  
235 to the rates expected from the measured composition. In order to derive the evaporation rates from the measured  
236 chemical composition of cooking SOA, we use the kinetic mass transfer model developed by Riipinen et al. (2010).

237 Among the inputs into the model, the mass accommodation coefficient is a critical but uncertain parameter that  
238 accounts for the mass transfer limitations in the system.

239 Figure 5 shows both measured and modeled mass thermograms for canola oil SOA. We observe that for canola oil  
240 SOA, mass accommodation coefficient of 0.03 is needed to predict the experimentally determined mass thermograms.  
241 An accommodation coefficient of  $<1$  suggests that mass transfer limitations in the system likely occurring in the  
242 condensed phase. Formation of multifunctional organic compounds such as those observed in this study is likely  
243 responsible for an increase in viscosity through increasing hydrogen bonding and other polar interactions (Rothfuss  
244 and Petters, 2016). It should be noted that Takhar et al. (2019) reported similar magnitudes of mass accommodation  
245 coefficients for heterogeneous oxidation of cooking oil particles. Due to similarity in the type of functional groups  
246 present in both aging pathways, we believe the decrease in mass accommodation coefficients for both systems undergo  
247 similar changes in phase and/or viscosity.

248 These measurements of evaporation rates are consistent with the volatilities expected from our measured composition  
249 of SOA containing small oxygenated compounds. Although mass accommodation coefficients are highly uncertain,  
250 the mass accommodation coefficients for other SOA systems have been measured to be even lower on the order of  $10^{-4}$   
251 (Cappa and Wilson, 2011), which would require the volatilities to be even higher to explain the measured evaporation  
252 rates. Therefore, the TD measurements support the conclusion that smaller oxygenated compounds are produced from  
253 oxidation of cooking oil vapors, and that fragmentation reactions are dominant. Furthermore, these measurements  
254 provide useful inputs into chemical transport models for predicting SOA formation and gas-particle partitioning. Our  
255 previous work (Takhar et al., 2019) showed that even at  $\alpha = 10^{-2}$ , gas-particle partitioning timescales are short (within  
256 hours) and the assumption of equilibrium partitioning still holds for regional scale SOA formation. Further work is  
257 needed to directly measure the viscosity of cooking SOA, and corresponding mixing timescales to better constrain the  
258 physicochemical properties of cooking SOA.

259

### 260 **3.3 Contribution of aldehydes to observed oxidation products and total SOA**

261 Since cooking oil vapors are comprised of a number of reactive aldehydes that can lead to SOA formation, we conduct  
262 further experiments of SOA formation from these precursors and identify the relative contributions to observed  
263 oxidation products and to total SOA. These results are applied to the heated cooking oil experiments to understand the  
264 role of aldehydes in the overall production and evolution of cooking oil SOA.

#### 265 **3.3.1 Formation of particle-phase oxidation products**

266 As described in the earlier sections, we are able to quantify the mass concentrations of different compound groups (6  
267 different combinations of functional groups, from C2 to C10, summarized in Table S2) in the particle phase for all  
268 experiments. We denote the observed mass concentrations of compound group  $i$  in SOA from canola oil  
269 photooxidation as  $M_i^{oil}$ . The expected precursors to these oxidation products are likely aldehydes, since aldehydes are



270 emitted in significant amounts and are highly reactive. To examine this hypothesis, here we calculate the formation  
271 of these observed compound groups from oxidation of aldehydes. For this calculation, heptanal, *trans*-2-heptenal,  
272 *trans*-2-octenal, *trans,trans*-2,4-heptadienal, and *trans,trans*-2,4-decadienal (Sigma Aldrich Co.) were considered  
273 because these aldehydes are the dominant VOC precursors emitted from heated canola oil in our experiments as shown  
274 in Fig. S8. More volatile aldehydes, such as acrolein and methacrolein, were likely present but could not be captured  
275 and analyzed by our techniques. The molar amount reacted for each aldehyde  $j$  in the canola oil oxidation experiments  
276 is denoted as  $\Delta VOC_j^{oil}$ , and was calculated based on the measured OH exposure.

277 In order to estimate the contribution from oxidation of an aldehyde  $j$  in the gas-phase mix to the formation of each  
278 compound group  $i$ , we conducted a series of experiments in which a representative aldehyde was oxidized, and the  
279 molar yields of the various compounds were measured:

$$280 \quad \gamma_{ij} = \frac{M_{ij}^{ind}/MW_i}{\Delta VOC_j^{ind}} \quad (3)$$

281 where  $\gamma_{ij}$  represents the molar yield of compound group  $i$  from precursor  $j$ ,  $M_{ij}^{ind}$  denotes the mass concentration of  
282 compound  $i$  observed in photooxidation experiments in which aldehyde  $j$  was the sole precursor,  $MW_i$  is the molecular  
283 weight of compound  $i$ , and  $\Delta VOC_j^{ind}$  is the amount of precursor  $j$  reacted in each experiment.  $\gamma_{ij}$  is then applied to the  
284 heated cooking oil experiments to estimate the amount of oxidation products that would form from each precursor:

$$285 \quad M_i^{sum} = \sum_j \gamma_{ij} \Delta VOC_j^{oil} MW_i \quad (4)$$

286 A sample calculation for this analysis is presented in Sect. 4 of SI. The comparison between  $M_i^{sum}$  (contribution of  
287 aldehyde oxidation to formation of compound  $i$ ) and  $M_i^{oil}$  (observed concentrations of compound  $i$ ) is shown in Fig.  
288 6. Based on this methodology, oxidation of aldehydes accounts for  $63 \mu\text{g m}^{-3}$  ( $M_i^{sum}$ ) of the observed  $75 \mu\text{g m}^{-3}$  ( $M_i^{oil}$ )  
289 (or 84%) particle-phase oxidation products measured at an OH exposure of  $6.43 \times 10^{10}$  molecules  $\text{cm}^{-3}$  s. The  
290 contributions of alkanals (heptanal), alkenals (heptenal + octenal) and alkadienals (heptadienal + decadienal) are 7%,  
291 ~31% and 46%, respectively.

292 While the amount of oxidation products expected from aldehydes is somewhat lower than that observed in canola oil  
293 SOA, this difference may arise from differences in gas-particle partitioning between single aldehyde photooxidation  
294 and canola oil photooxidation. As shown in Fig. 6, the formation of higher carbon # products cannot be explained  
295 from the photooxidation of aldehydes used to predict oil oxidation products likely due to the assumption of negligible  
296 particle-phase or oligomerization reactions occurring in the condensed phase. In addition, higher carbon # acids are  
297 likely present as primary vapors in the gas phase which can then partition to the condensed phase upon SOA formation.  
298 As shown in Fig. S9, more oxygenated compounds (higher O:C and greater number of functional groups) tend to be  
299 more abundant in the canola oil SOA than expected from aldehyde photooxidation, suggesting that canola oil SOA is  
300 more favorable for oxygenated compounds to partition than SOA from individual aldehydes. On the other hand, there  
301 is no clear trend in partitioning with respect to vapor pressures and carbon number. It should be noted that uncertainties

302 in the fitting procedure or estimation in the pseudo molecular ion (refer to Table S2 and Fig. S5) can also result in  
303 uncertainties between -40% and +20%. Therefore, in summary, the quantified oxidation products from canola oil SOA  
304 are generally consistent with those from aldehyde photooxidation, and the relative amounts may be subject to further  
305 changes due to gas-particle partitioning.

306

### 307 3.3.2 Using the statistical oxidation model (SOM) framework

308 To further explore the evolution of canola oil SOA, we applied our results to the statistical oxidation model (SOM)  
309 framework developed by Cappa and Wilson (Cappa et al., 2013; Cappa and Wilson, 2012). SOM describes the  
310 oxidation chemistry of a VOC precursor through multi-generational space defined by the number of carbon and  
311 oxygen atoms present in the precursor and its possible SOA product molecules. The SOM does not specifically track  
312 the product composition in terms of functional groups, but provides adequate details to represent key atmospheric  
313 processes such as gas-particle partitioning, fragmentation, functionalization, reactions with oxidants, condensed-phase  
314 chemistry. The model has been applied to chamber experiments to derive parametrizations by fitting experimental  
315 data to both SOA mass concentration and the bulk aerosol O/C ratio. Eluri et al. (2018) used the chamber derived  
316 parameterizations to predict the properties of SOA generated from diesel exhaust in an oxidation flow tube reactor.

317 To the best of the authors' knowledge, there are no parameterizations for the oxidation of aldehydes. Therefore, in  
318 this study we first derived the parameterizations for aldehyde oxidation, and then use these parameters to predict the  
319 SOA mass concentrations. In order to obtain the parameters, we fit the measured SOA concentration from oxidation  
320 of heptanal, *trans*-2-heptenal, *trans,trans*-2,4-heptadienal at different OH exposures to optimize the six tunable  
321 parameters under low-NO<sub>x</sub> conditions (shown in Fig. S10). Best fit SOM parameters indicate that photooxidation  
322 leads to fragmentation per reaction with OH, as shown by a lower *mfrag* than compared to other systems e.g. alkanes  
323 ( $\geq 2$  for branched, cyclic or *n*-alkane under low-NO<sub>x</sub> conditions (Eluri et al., 2018)). Since a lower value for *mfrag*  
324 represents greater fragmentation (Cappa and Wilson, 2012), this again reflects the higher propensity for fragmentation  
325 in this SOA system. The optimized parameters were then used to predict the SOA concentration for canola oil  
326 photooxidation under different aging conditions in the OH exposure range similar to that of aldehyde photooxidation.

327 Based on these established parameterizations for different aldehydes, model simulations were conducted for canola  
328 oil having a mixture of aldehydes under different photochemical aging conditions. It should be noted that we used  
329 parameterizations of heptanal for all alkanals, heptenal for all alkenals, and heptadienal for alkadienals. As shown in  
330 Fig. 7, the model generally captures the amount of SOA formed to up to 62%, but overpredicts SOA formation at  
331 lower photochemical ages and underpredicts SOA concentrations at higher photochemical ages. In addition, SOM  
332 also tracks atomic O/C ratio which were further compared with the measured O/C ratio. SOM predicts an O:C around  
333 0.51, which is within 50% of the measured O:C likely suggesting that the changes in chemical composition of cooking  
334 SOA is in a reasonable agreement with the model predictions. Furthermore, the unexplained SOA can likely arise  
335 from other unidentified S/IVOCs as hypothesized by Liu et al. (2017c). However, unlike traffic emissions (Zhao et

336 al., 2014), S/IVOCs from cooking has not been positively identified. In addition, small VOC precursors like acrolein  
337 and malondialdehyde which have been measured in large quantities from cooking emissions (Klein et al., 2016a), may  
338 form SOA products having higher O/C ratios, which may better explain the O/C ratios observed in our experiments.

339 One inconsistency between the model and measurements is the slope at which SOA is being formed. The experimental  
340 data suggest a steeper trend of SOA formation while the model predicts a more gradual increase in SOA formation. A  
341 potential explanation for this discrepancy is the contribution from other unmeasured VOCs. These VOCs are less  
342 reactive than those considered in the model, such that they contribute to higher SOA at higher OH exposures.  
343 Alternatively, these missing VOCs are more volatile such that more of their SOA is formed at later generations of  
344 oxidation. For example, acrolein forms SOA with measurable yields (Chan et al., 2010) and is emitted at large amounts  
345 from heated cooking oils (Klein et al., 2016a). Despite these limitations, these parameterizations generally capture the  
346 amount of SOA formed and its degree of oxidation (O/C) on oxidation timescales relevant to urban areas (within 2  
347 days) and are useful for representing cooking oil emissions in the chemical transport models. Overall, the amount of  
348 SOA formed and the evolution upon oxidation can be well described by photooxidation of aldehydes.

349

#### 350 **4 Conclusions and implications**

351 In this work, we characterized the detailed chemical composition of SOA generated from cooking oil vapors. We  
352 showed that cooking SOA occurring as highly complex mixture can be deconvoluted using mass spectral  
353 fragmentation pattern to extract useful information about the chemical identities of organic compounds, such as  
354 functional groups and carbon number. Using this detailed chemical composition of cooking SOA, we showed that  
355 fragmentation is an important pathway for oxidative processing of cooking emissions in the atmosphere even within  
356 short timescales of oxidation. Furthermore, we showed that aldehydes can reasonably explain the formation of SOA  
357 generated from cooking oil vapors and the oxidative evolution as described using a multi-generational oxidation  
358 model. Our study, therefore, highlights the importance of molecular composition in constraining the chemical  
359 properties of cooking SOA, as well as understanding the contribution of aldehydes in formation of SOA from cooking  
360 emissions.

361 Consistent with other studies, our work has shown that aldehydes are an important class of VOC precursors emitted  
362 from cooking emissions, and substantial efforts have been made to measure their emission factors depending on  
363 different cooking settings (heating temperature, cooking style, food, ingredients) (Klein et al., 2016a, 2016b).  
364 However, the contribution of aldehydes from cooking emissions is underrepresented in chemical transport models.  
365 Recently, McDonald et al. (2018) showed that the ambient concentrations of OA were underpredicted when aldehydes  
366 were not included in the box model calculations, suggesting that aldehydes, likely from food cooking, play an  
367 important role in atmospheric oxidation chemistry. Furthermore, Klein et al. (2019) showed that heavy pollutants like  
368 restaurants play a significant role in contributing to the ambient cooking organic aerosol concentrations. In this study,  
369 we showed a large fraction of the SOA is derived from aldehyde precursors, with strong similarities in chemical  
370 composition. Therefore, it is important to consider the contribution of aldehyde chemistry in atmospheric models

371 towards total OA budget. Furthermore, we demonstrated the importance of fragmentation reactions and their influence  
372 on OA properties such as volatility and chemical composition. Future work should therefore focus on measuring not  
373 only the SOA formation, but also the oxygenated VOCs formed due to fragmentation upon aging to provide insights  
374 into aging of cooking emissions.

375 Formation of SOA from cooking emissions in the atmosphere is likely influenced by emissions of POA, and other  
376 gas-phase precursors. Therefore, inclusion of POA during atmospheric processing of cooking emissions will likely  
377 influence the physicochemical properties of cooking SOA. For instance, with cooking POA being much less  
378 functionalized than SOA, inclusion of POA will likely decrease the system O:C (or  $\overline{O:C}$ ). However, POA from  
379 cooking emissions can undergo heterogeneous reactions in the atmosphere, thereby increasing O:C (or  $\overline{O:C}$ ). On the  
380 other hand, there could potentially be contributions from other gas-phase precursors or S/IVOCs emitted from cooking  
381 vapors that can result in SOA formation. These precursors can potentially contribute to SOA formation from cooking  
382 emissions, but their oxidative evolution in the atmosphere is not well understood.

383 Gas-particle partitioning of SOA can be further affected by non-ideal mixing, as well as morphology of the particles  
384 (Shiraiwa et al., 2013; Zuend and Seinfeld, 2012). Future work should investigate the effect of these parameters on  
385 cooking SOA properties and formation potential. To account for thermodynamic mixing favourability of the particles,  
386 Hansen solubility framework developed by Ye et al. (2016) can be implemented to provide insights into SOA mixing  
387 and yield enhancement. As shown in Ye et al. (2018) primary meat-cooking emissions can enhance SOA yield from  
388  $\alpha$ -pinene due to similarity in Hansen solubility parameters suggesting that primary meat cooking particles are miscible  
389 with  $\alpha$ -pinene SOA. It should be noted that present study did not investigate the effect of atmospherically relevant  
390 seed particles as well as  $\text{NO}_x$  levels which are representative of typical urban environments. Since emissions upon  
391 entering the atmosphere gets mixed with background air, other source emissions, and diluted upon mixing thereby  
392 altering the gas-particle partitioning, and thus the total OA loading. Therefore, it is important to understand the changes  
393 in partitioning and miscibility of cooking emissions as the composition continually evolves with atmospheric  
394 processing. Additionally, as mentioned earlier cooking SOA undergoes large mass transfer limitations due to changes  
395 in the phase state of the SOA particles, making it more so important to experimentally determine the corresponding  
396 viscosity of cooking SOA. Therefore, future work should focus on measuring both the viscosity and miscibility of  
397 SOA derived from cooking emissions.

398

399 *Data availability.* The data are available upon request to the corresponding author.

400

401 *Author Contributions.* MT and AWHC designed research. MT collected and analyzed data. MT, YL and AWHC  
402 interpreted results. MT and AWHC wrote the manuscript with inputs from YL.

403

404 *Competing interests.* The authors declare that they have no conflict of interests.

405

406 *Acknowledgements.* The authors acknowledge Environment and Climate Change Canada (ECCC) for funding support  
407 through the Government of Canada Grants and Contribution program. The authors would like to thank Shao-Meng Li  
408 from ECCC for use of the thermodenuder, Chris Cappa from UC Davis for help with SOM simulations, Greg Evans,  
409 Jeff Brook and Tengyu Liu from University of Toronto for helpful discussion.

410 **References**

- 411 Allan, J. D., Williams, P. I., Morgan, W. T., Martin, C. L., Flynn, M. J., Lee, J., Nemitz, E., Phillips, G. J.,  
412 Gallagher, M. W. and Coe, H.: Contributions from transport, solid fuel burning and cooking to primary organic  
413 aerosols in two UK cities, *Atmos. Chem. Phys.*, 10(2), 647–668, doi:10.5194/acp-10-647-2010, 2010.
- 414 Canagaratna, M. R., Jimenez, J. L., Kroll, J. H., Chen, Q., Kessler, S. H., Massoli, P., Hildebrandt Ruiz, L., Fortner,  
415 E., Williams, L. R., Wilson, K. R., Surratt, J. D., Donahue, N. M., Jayne, J. T. and Worsnop, D. R.: Elemental ratio  
416 measurements of organic compounds using aerosol mass spectrometry: Characterization, improved calibration, and  
417 implications, *Atmos. Chem. Phys.*, 15(1), 253–272, doi:10.5194/acp-15-253-2015, 2015.
- 418 Cappa, C. D. and Wilson, K. R.: Evolution of organic aerosol mass spectra upon heating: Implications for OA phase  
419 and partitioning behavior, *Atmos. Chem. Phys.*, 11(5), 1895–1911, doi:10.5194/acp-11-1895-2011, 2011.
- 420 Cappa, C. D. and Wilson, K. R.: Multi-generation gas-phase oxidation, equilibrium partitioning, and the formation  
421 and evolution of secondary organic aerosol, *Atmos. Chem. Phys.*, 12(20), 9505–9528, doi:10.5194/acp-12-9505-  
422 2012, 2012.
- 423 Cappa, C. D., Zhang, X., Loza, C. L., Craven, J. S., Yee, L. D. and Seinfeld, J. H.: Application of the Statistical  
424 Oxidation Model (SOM) to Secondary Organic Aerosol formation from photooxidation of C12 alkanes, *Atmos.*  
425 *Chem. Phys.*, 13(3), 1591–1606, doi:10.5194/acp-13-1591-2013, 2013.
- 426 Chan, A. W. H., Chan, M. N., Surratt, J. D., Chhabra, P. S., Loza, C. L., Crouse, J. D., Yee, L. D., Flagan, R. C.,  
427 Wennberg, P. O. and Seinfeld, J. H.: Role of aldehyde chemistry and NO<sub>x</sub> concentrations in secondary organic  
428 aerosol formation, *Atmos. Chem. Phys.*, 10(15), 7169–7188, doi:10.5194/acp-10-7169-2010, 2010.
- 429 Choe, E. and Min, D. B.: Mechanisms and factors for edible oil oxidation, *Compr. Rev. Food Sci. Food Saf.*, 5(4),  
430 169–186, doi:10.1111/j.1541-4337.2006.00009.x, 2006.
- 431 Choe, E. and Min, D. B.: Chemistry of deep-fat frying oils, *J. Food Sci.*, 72(5), doi:10.1111/j.1750-  
432 3841.2007.00352.x, 2007.
- 433 Crippa, M., Decarlo, P. F., Slowik, J. G., Mohr, C., Heringa, M. F., Chirico, R., Poulain, L., Freutel, F., Sciare, J.,  
434 Cozic, J., Di Marco, C. F., Elsasser, M., Nicolas, J. B., Marchand, N., Abidi, E., Wiedensohler, A., Drewnick, F.,  
435 Schneider, J., Borrmann, S., Nemitz, E., Zimmermann, R., Jaffrezou, J.-L., Prevot, A. S. H. and Baltensperger, U.:  
436 Wintertime aerosol chemical composition and source apportionment of the organic fraction in the metropolitan area  
437 of Paris, *Atmos. Chem. Phys.*, 13(2), 961–981, doi:10.5194/acp-13-961-2013, 2013.
- 438 Dall’Osto, M., Paglione, M., Decesari, S., Facchini, M. C., O’Dowd, C., Plass-Duellmer, C. and Harrison, R. M.: On  
439 the Origin of AMS “cooking Organic Aerosol” at a Rural Site, *Environ. Sci. Technol.*, 49(24), 13964–13972,  
440 doi:10.1021/acs.est.5b02922, 2015.
- 441 Donahue, N. M., Robinson, A. L., Stanier, C. O. and Pandis, S. N.: Coupled partitioning, dilution, and chemical  
442 aging of semivolatile organics, *Environ. Sci. Technol.*, 40(8), 2635–2643, doi:10.1021/es052297c, 2006.
- 443 Donahue, N. M., Kroll, J. H., Pandis, S. N. and Robinson, A. L.: A two-dimensional volatility basis set-Part 2:  
444 Diagnostics of organic-aerosol evolution, *Atmos. Chem. Phys.*, 12(2), 615–634, doi:10.5194/acp-12-615-2012,  
445 2012.
- 446 Eluri, S., Cappa, C. D., Friedman, B., Farmer, D. K. and Jathar, S. H.: Modeling the formation and composition of  
447 secondary organic aerosol from diesel exhaust using parameterized and semi-explicit chemistry and thermodynamic  
448 models, *Atmos. Chem. Phys.*, 18(19), 13813–13838, doi:10.5194/acp-18-13813-2018, 2018.
- 449 Florou, K., Papanastasiou, D. K., Pikridas, M., Kaltsonoudis, C., Louvaris, E., Gkatzelis, G. I., Patoulias, D.,  
450 Mihalopoulos, N. and Pandis, S. N.: The contribution of wood burning and other pollution sources to wintertime  
451 organic aerosol levels in two Greek cities, *Atmos. Chem. Phys.*, 17(4), 3145–3163, doi:10.5194/acp-17-3145-2017,  
452 2017.

453 Fullana, A., Carbonell-Barrachina, A. A. and Sidhu, S.: Comparison of volatile aldehydes present in the cooking  
454 fumes of extra virgin olive, olive, and canola oils, *J. Agric. Food Chem.*, 52(16), 5207–5214, doi:10.1021/jf035241f,  
455 2004a.

456 Fullana, A., Carbonell-Barrachina, A. A. and Sidhu, S.: Volatile aldehyde emissions from heated cooking oils, *J.*  
457 *Sci. Food Agric.*, 84(15), 2015–2021, doi:10.1002/jsfa.1904, 2004b.

458 Gardner, H. W.: Oxygen radical chemistry of polyunsaturated fatty acids, *Free Radic. Biol. Med.*, 7(1), 65–86,  
459 doi:10.1016/0891-5849(89)90102-0, 1989.

460 Hallquist, M., Wenger, J. C., Baltensperger, U., Rudich, Y., Simpson, D., Claeys, M., Dommen, J., Donahue, N. M.,  
461 George, C., Goldstein, A. H., Hamilton, J. F., Herrmann, H., Hoffmann, T., Iinuma, Y., Jang, M., Jenkin, M. E.,  
462 Jimenez, J. L., Kiendler-Scharr, J., Maenhaut, W., McFiggans, G., Mentel, T. F., Monod, A., Prevot, A. S. H.,  
463 Seinfeld, J. H., Surratt, J. D., Szmigielski, R. and Wildt, J.: The formation, properties and impact of secondary  
464 organic aerosol: current and emerging issues, *Atmos. Chem. Phys.*, 9(14), 5155–5236, doi:10.5194/acp-9-5155-  
465 2009, 2009.

466 Hayes, P. L., Ortega, A. M., Cubison, M. J., Froyd, K. D., Zhao, Y., Cliff, S. S., Hu, W. W., Toohey, D. W., Flynn,  
467 J. H., Lefter, B. L., Grossberg, N., Alvarez, S., Rappenglück, B., Taylor, J. W., Allan, J. D., Holloway, J. S., Gilman,  
468 J. B., Kuster, W. C., De Gouw, J. A., Massoli, P., Zhang, X., Liu, J., Weber, R. J., Corrigan, A. L., Russell, L. M.,  
469 Isaacman, G., Worton, D. R., Kreisberg, N. M., Goldstein, A. H., Thalman, R., Waxman, E. M., Volkamer, R., Lin,  
470 Y. H., Surratt, J. D., Kleindienst, T. E., Offenberg, J. H., Dusanter, S., Griffith, S., Stevens, P. S., Brioude, J.,  
471 Angevine, W. M. and Jimenez, J. L.: Organic aerosol composition and sources in Pasadena, California, during the  
472 2010 CalNex campaign, *J. Geophys. Res. Atmos.*, 118(16), 9233–9257, doi:10.1002/jgrd.50530, 2013.

473 Heald, C. L., Kroll, J. H., Jimenez, J. L., Docherty, K. S., Decarlo, P. F., Aiken, A. C., Chen, Q., Martin, S. T.,  
474 Farmer, D. K. and Artaxo, P.: A simplified description of the evolution of organic aerosol composition in the  
475 atmosphere, *Geophys. Res. Lett.*, 37(8), doi:10.1029/2010GL042737, 2010.

476 Huang, X., He, L., Hu, M., Canagaratna, M. R., Sun, Y., Zhang, Q., Zhu, T., Xue, L., Zeng, L. W., Liu, X. G.,  
477 Zhang, Y. H., Jayne, J. T., Ng, N. L. and Worsnop, D. R.: and Physics Highly time-resolved chemical  
478 characterization of atmospheric submicron particles during 2008 Beijing Olympic Games using an Aerodyne High-  
479 Resolution Aerosol Mass Spectrometer, *Atmos. Chem. Phys.*, 10(18), 8933–8945, doi:10.5194/acp-10-8933-2010,  
480 2010.

481 Isaacman-VanWertz, G., Lu, X., Weiner, E., Smiley, E. B. and Widdowson, M. A.: Characterization of hydrocarbon  
482 groups in complex mixtures using gas chromatography with unit-mass resolution electron ionization mass  
483 spectrometry, *Anal. Chem.*, 92(18), 12481–12488, doi:10.1021/acs.analchem.0c02308, 2020.

484 Jaoui, M., Kleindienst, T. E., Lewandowski, M. and Edney, E. O.: Identification and quantification of aerosol polar  
485 oxygenated compounds bearing carboxylic or hydroxyl groups. 1. Method development, *Anal. Chem.*, 76(16),  
486 4765–4778, doi:10.1021/ac049919h, 2004.

487 Jaoui, M., Kleindienst, T. E., Lewandowski, M., Offenberg, J. H. and Edney, E. O.: Identification and quantification  
488 of aerosol polar oxygenated compounds bearing carboxylic or hydroxyl groups. 2. Organic tracer compounds from  
489 monoterpenes, *Environ. Sci. Technol.*, 39(15), 5661–5673, doi:10.1021/es048111b, 2005.

490 Kaltsonoudis, C., Kostenidou, E., Louvaris, E., Psichoudaki, M., Tsiligiannis, E., Florou, K., Liangou, A. and  
491 Pandis, S. N.: Characterization of fresh and aged organic aerosol emissions from meat charbroiling, *Atmos. Chem.*  
492 *Phys.*, 17(11), 7143–7155, doi:10.5194/acp-17-7143-2017, 2017.

493 Katragadda, H. R., Fullana, A., Sidhu, S. and Carbonell-Barrachina, A. A.: Emissions of volatile aldehydes from  
494 heated cooking oils, *Food Chem.*, 120(1), 59–65, doi:10.1016/j.foodchem.2009.09.070, 2010.

495 Klein, F., Platt, S. M., Farren, N. J., Detournay, A., Bruns, E. A., Bozzetti, C., Daellenbach, K. R., Kilic, D., Kumar,  
496 N. K., Pieber, S. M., Slowik, J. G., Temime-roussel, B., Marchand, N., Hamilton, J. F., Baltensperger, U., Prévôt, A.  
497 S. H. and El Haddad, I.: Characterization of Gas-Phase Organics Using Proton Transfer Reaction Time-of-Flight

498 Mass Spectrometry: Cooking Emissions, *Environ. Sci. Technol.*, 50(3), 1243–1250, doi:10.1021/acs.est.5b04618,  
499 2016a.

500 Klein, F., Farren, N. J., Bozzetti, C., Daellenbach, K. R., Kilic, D., Kumar, N. K., Pieber, S. M., Slowik, J. G.,  
501 Tuthill, R. N., Hamilton, J. F., Baltensperger, U., Prévôt, A. S. H. and El Haddad, I.: Indoor terpene emissions from  
502 cooking with herbs and pepper and their secondary organic aerosol production potential, *Sci. Rep.*, 6, 1–7,  
503 doi:10.1038/srep36623, 2016b.

504 Klein, F., Baltensperger, U., Prévôt, A. S. H. and El Haddad, I.: Quantification of the impact of cooking processes  
505 on indoor concentrations of volatile organic species and primary and secondary organic aerosols, *Indoor Air*, 29(6),  
506 926–942, doi:10.1111/ina.12597, 2019.

507 Kostenidou, E., Florou, K., Kaltsonoudis, C., Tsiflikiotou, M., Vratolis, S., Eleftheriadis, K. and Pandis, S. N.:  
508 Sources and chemical characterization of organic aerosol during the summer in the eastern Mediterranean, *Atmos.*  
509 *Chem. Phys.*, 15(19), 11355–11371, doi:10.5194/acp-15-11355-2015, 2015.

510 Kroll, J. H., Donahue, N. M., Jimenez, J. L., Kessler, S. H., Canagaratna, M. R., Wilson, K. R., Altieri, K. E.,  
511 Mazzoleni, L. R., Wozniak, A. S., Bluhm, H., Mysak, E. R., Smith, J. D., Kolb, C. E. and Worsnop, D. R.: Carbon  
512 oxidation state as a metric for describing the chemistry of atmospheric organic aerosol, *Nat. Chem.*, 3(2), 133–139,  
513 doi:10.1038/nchem.948, 2011.

514 Lee, B. P., Li, Y. J., Yu, J. Z., Louie, P. K. K. and Chan, C. K.: Characteristics of submicron particulate matter at the  
515 urban roadside in downtown Hong Kong—overview of 4 months of continuous high-resolution aerosol mass  
516 spectrometer measurements, *J. Geophys. Res.*, 120(14), 7040–7058, doi:10.1002/2015JD023311. Received, 2015.

517 Liu, T., Liu, Q., Li, Z., Huo, L., Chan, M. N., Li, X., Zhou, Z. and Chan, C. K.: Emission of volatile organic  
518 compounds and production of secondary organic aerosol from stir-frying spices, *Sci. Total Environ.*, 599–600,  
519 1614–1621, doi:10.1016/j.scitotenv.2017.05.147, 2017a.

520 Liu, T., Li, Z., Chan, M. and Chan, C. K.: Formation of secondary organic aerosols from gas-phase emissions of  
521 heated cooking oils, *Atmos. Chem. Phys.*, 17(12), 7333–7344, doi:10.5194/acp-17-7333-2017, 2017b.

522 Liu, T., Wang, Z., Huang, D. D., Wang, X. and Chan, C. K.: Significant Production of Secondary Organic Aerosol  
523 from Emissions of Heated Cooking Oils, *Environ. Sci. Technol. Lett.*, 5(1), 32–37, doi:10.1021/acs.estlett.7b00530,  
524 2017c.

525 Liu, T., Wang, Z., Wang, X. and Chan, C. K.: Primary and secondary organic aerosol from heated cooking oil  
526 emissions, *Atmos. Chem. Phys.*, 18(15), 11363–11374, doi:10.5194/acp-18-11363-2018, 2018.

527 Lopez-Hilfiker, F. D., Pospisilova, V., Huang, W., Kalberer, M., Mohr, C., Stefenelli, G., Thornton, J. A.,  
528 Baltensperger, U., Prevot, A. S. H. and Slowik, J. G.: An Extractive Electrospray Ionization Time-of-Flight Mass  
529 Spectrometer (EESI-TOF) for online measurement of atmospheric aerosol particles, *Atmos. Meas. Tech.*, 12(9), 1–  
530 40, doi:10.5194/amt-2019-45, 2019.

531 Mao, J., Ren, X., Brune, W. H., Olson, J. R., Crawford, J. H., Fried, A., Huey, L. G., Cohen, R. C., Heikes, B.,  
532 Singh, H. B., Blake, D. R., Sachse, G. W., Diskin, G. S., Hall, S. R. and Shetter, R. E.: Airborne measurement of  
533 OH reactivity during INTEX-B, *Atmos. Chem. Phys.*, 9(1), 163–173, doi:10.5194/acp-9-163-2009, 2009.

534 McDonald, B. C., De Gouw, J. A., Gilman, J. B., Jathar, S. H., Akherati, A., Cappa, C. D., Jimenez, J. L., Lee-  
535 Taylor, J., Hayes, P. L., McKeen, S. A., Cui, Y. Y., Kim, S. W., Gentner, D. R., Isaacman-VanWertz, G., Goldstein,  
536 A. H., Harley, R. A. and Frost, M.: Volatile chemical products emerging as largest petrochemical source of urban  
537 organic emissions, *Science* (80-. ), 359(6377), 760–764, doi:10.1126/science.aaq0524, 2018.

538 Mohr, C., Huffman, J. A., Cubison, M. J., Aiken, A. C., Docherty, K. S., Kimmel, J. R., Ulbrich, I. M., Hannigan,  
539 M. and Jimenez, J. L.: Characterization of primary organic aerosol emissions from meat cooking, trash burning, and  
540 motor vehicles with high-resolution aerosol mass spectrometry and comparison with ambient and chamber  
541 observations, *Environ. Sci. Technol.*, 43(7), 2443–2449, doi:10.1021/es8011518, 2009.



542 Mohr, C., Decarlo, P. F., Heringa, M. F., Chirico, R., Slowik, J. G., Richter, R., Reche, C., Alastuey, A., Querol, X.,  
543 Seco, R., Penuelas, J., Jimenez, J. L., Crippa, M., Zimmermann, R., Baltensperger, U. and Prévôt, A. S. H.:  
544 Identification and quantification of organic aerosol from cooking and other sources in Barcelona using aerosol mass  
545 spectrometer data, *Atmos. Chem. Phys.*, 12(4), 1649–1665, doi:10.5194/acp-12-1649-2012, 2012.

546 Pankow, J. F. and Asher, W. E.: SIMPOL.1: A simple group contribution method for predicting vapor pressures and  
547 enthalpies of vaporization of multifunctional organic compounds, *Atmos. Chem. Phys.*, 8(10), 2773–2796,  
548 doi:10.5194/acp-8-2773-2008, 2008.

549 Riipinen, I., Pierce, J. R., Donahue, N. M. and Pandis, S. N.: Equilibration time scales of organic aerosol inside  
550 thermodenuders: Evaporation kinetics versus thermodynamics, *Atmos. Environ.*, 44(5), 597–607,  
551 doi:10.1016/j.atmosenv.2009.11.022, 2010.

552 Rothfuss, N. E. and Petters, M. D.: Influence of functional groups on the viscosity of organic aerosol, *Environ. Sci.*  
553 *Technol.*, 51(1), 271–279, doi:10.1021/acs.est.6b04478, 2016.

554 Schauer, J. J., Kleeman, M. J., Cass, G. R. and Simoneit, B. R. T.: Measurement of emissions from air pollution  
555 sources. 1. C1 through C29 organic compounds from meat charbroiling, *Environ. Sci. Technol.*, 33(10), 1566–1577,  
556 doi:10.1021/es980076j, 1999.

557 Schauer, J. J., Kleeman, M. J., Cass, G. R. and Simoneit, B. R. T.: Measurement of emissions from air pollution  
558 sources. 4. C1-C27 organic compounds from cooking with seed oils, *Environ. Sci. Technol.*, 36(4), 567–575,  
559 doi:10.1021/es002053m, 2002.

560 Shiraiwa, M., Zuend, A., Bertram, A. K. and Seinfeld, J. H.: Gas-particle partitioning of atmospheric aerosols:  
561 Interplay of physical state, non-ideal mixing and morphology, *Phys. Chem. Chem. Phys.*, 15(27), 11441–11453,  
562 doi:10.1039/c3cp51595h, 2013.

563 Sun, Y.-L., Zhang, Q., Schwab, J. J., Demerjian, K. L., Chen, W.-N., Bae, M.-S., Hung, H.-M., Hogrefe, O., Frank,  
564 B., Rattigan, O. V. and Lin, Y.-C.: Characterization of the sources and processes of organic and inorganic aerosols  
565 in New York city with a high-resolution time-of-flight aerosol mass spectrometer, *Atmos. Chem. Phys.*, 11(4),  
566 1581–1602, doi:10.5194/acp-11-1581-2011, 2011.

567 Takhar, M., Stroud, C. A. and Chan, A. W. H.: Volatility Distribution and Evaporation Rates of Organic Aerosol  
568 from Cooking Oils and their Evolution upon Heterogeneous Oxidation, *ACS Earth Sp. Chem.*, 3(9), 1717–1728,  
569 doi:10.1021/acsearthspacechem.9b00110, 2019.

570 Ye, J., Gordon, C. A. and Chan, A. W. H.: Enhancement in Secondary Organic Aerosol Formation in the Presence  
571 of Preexisting Organic Particle, *Environ. Sci. Technol.*, 50(7), 3572–3579, doi:10.1021/acs.est.5b05512, 2016.

572 Ye, J., Van Rooy, P., Adam, C. H., Jeong, C. H., Urch, B., Cocker, D. R., Evans, G. J. and Chan, A. W. H.:  
573 Predicting Secondary Organic Aerosol Enhancement in the Presence of Atmospherically Relevant Organic Particles,  
574 *ACS Earth Sp. Chem.*, 2(10), 1035–1046, doi:10.1021/acsearthspacechem.8b00093, 2018.

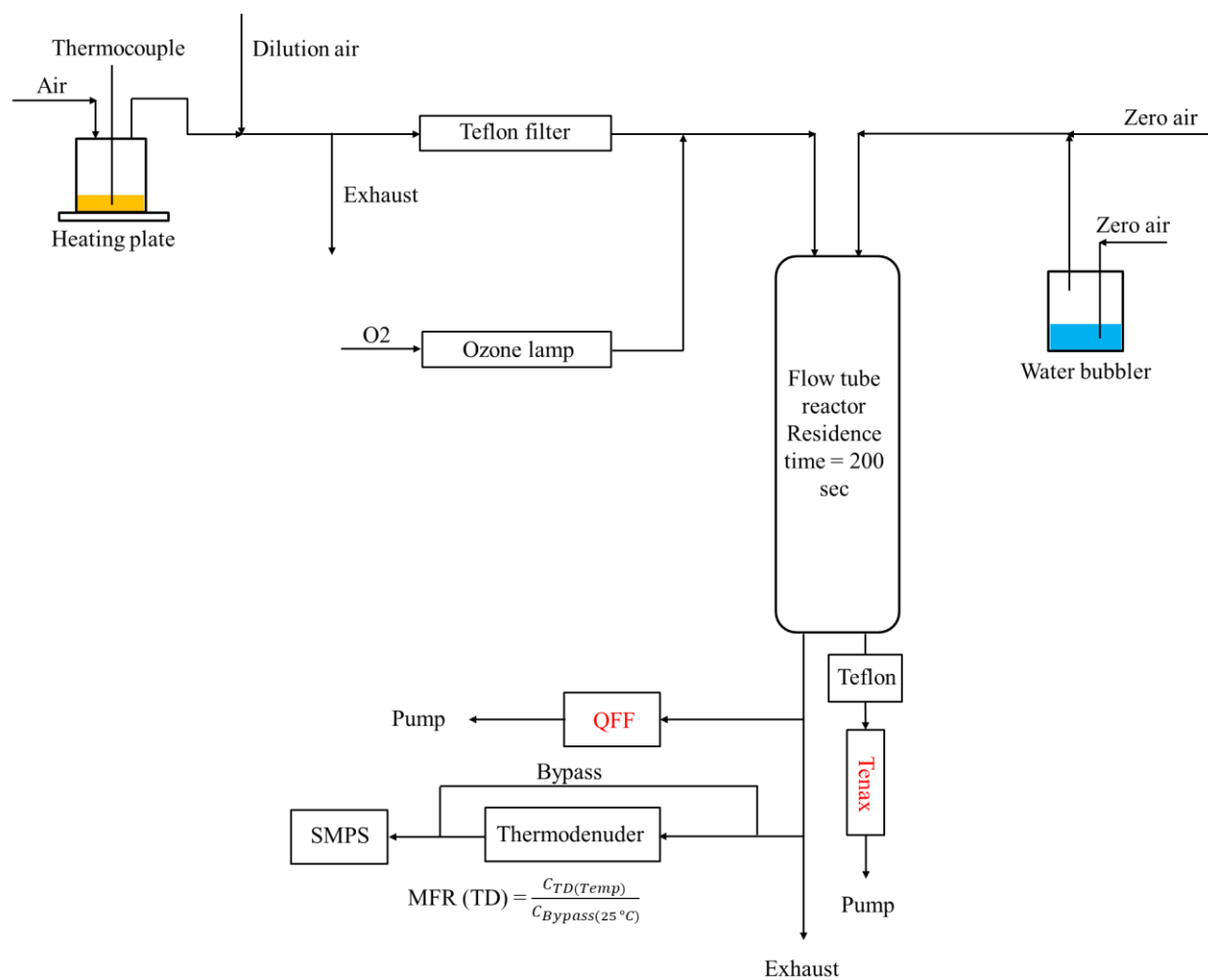
575 Yu, J., Flagan, R. C. and Seinfeld, J. H.: Identification of products containing -COOH, -OH, and -C=O in  
576 atmospheric oxidation of hydrocarbons, *Environ. Sci. Technol.*, 32(16), 2357–2370, doi:10.1021/es980129x, 1998.

577 Zhao, Y., Hennigan, C. J., May, A. A., Tkacik, D. S., De Gouw, J. A., Gilman, J. B., Kuster, W. C., Borbon, A. and  
578 Robinson, A. L.: Intermediate-volatility organic compounds: A large source of secondary organic aerosol, *Environ.*  
579 *Sci. Technol.*, 48(23), 13743–13750, doi:10.1021/es5035188, 2014.

580 Zhao, Y., Nguyen, N. T., Presto, A. A., Hennigan, C. J., May, A. A. and Robinson, A. L.: Intermediate Volatility  
581 Organic Compound Emissions from On-Road Diesel Vehicles: Chemical Composition, Emission Factors, and  
582 Estimated Secondary Organic Aerosol Production, *Environ. Sci. Technol.*, 49(19), 11516–11526,  
583 doi:10.1021/acs.est.5b02841, 2015.

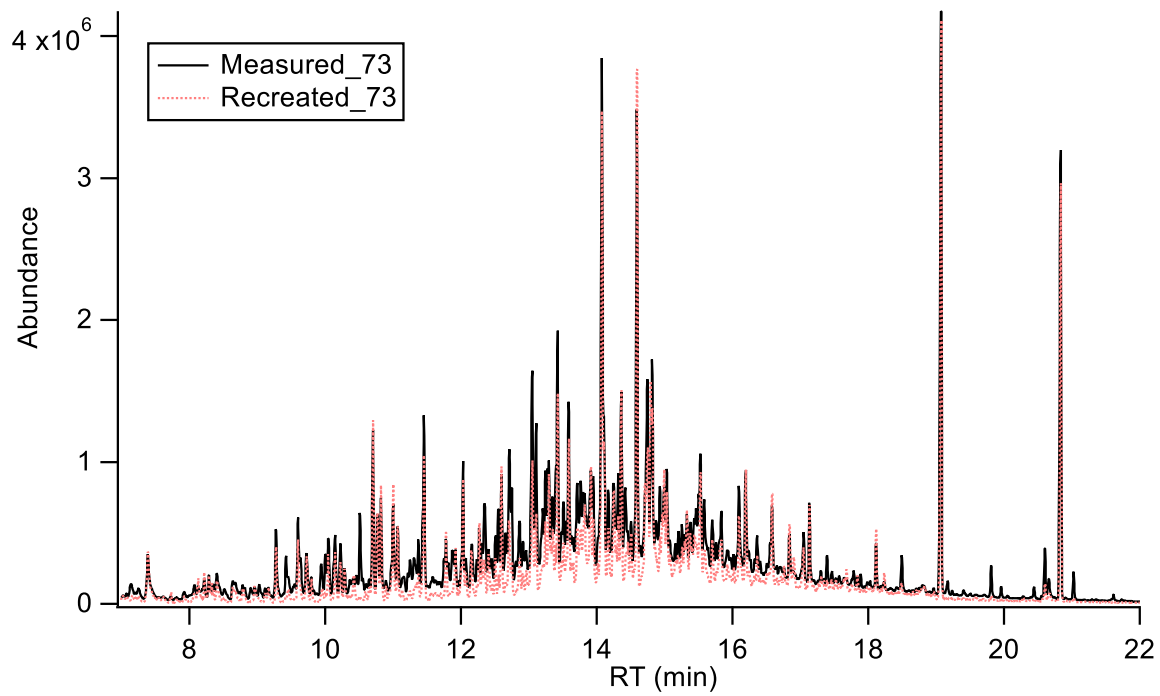
584 Zuend, A. and Seinfeld, J. H.: Modeling the gas-particle partitioning of secondary organic aerosol: The importance  
585 of liquid-liquid phase separation, *Atmos. Chem. Phys.*, 12(9), 3857–3882, doi:10.5194/acp-12-3857-2012, 2012.

586



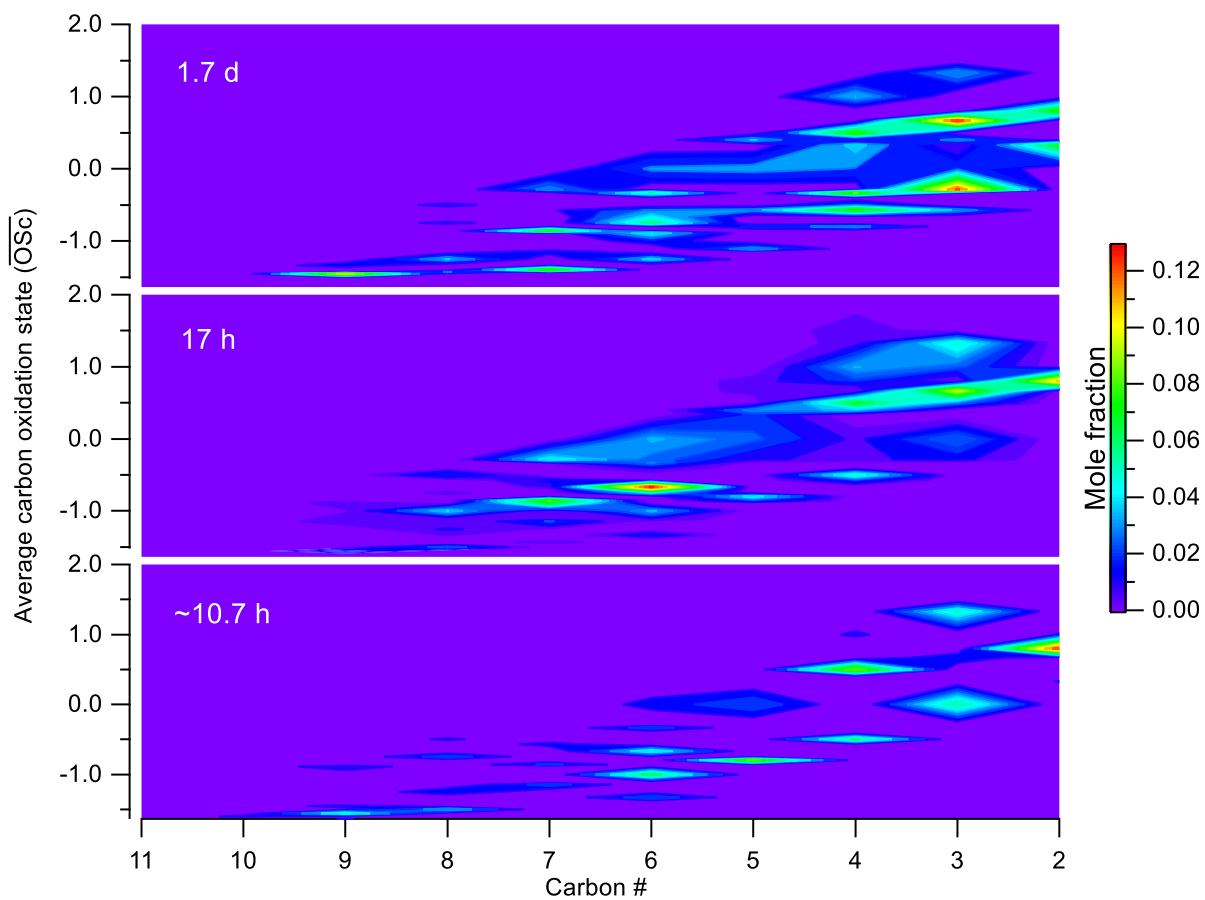
587

588 **Figure 1.** Experimental setup for oxidation of heated cooking oil emissions.



589

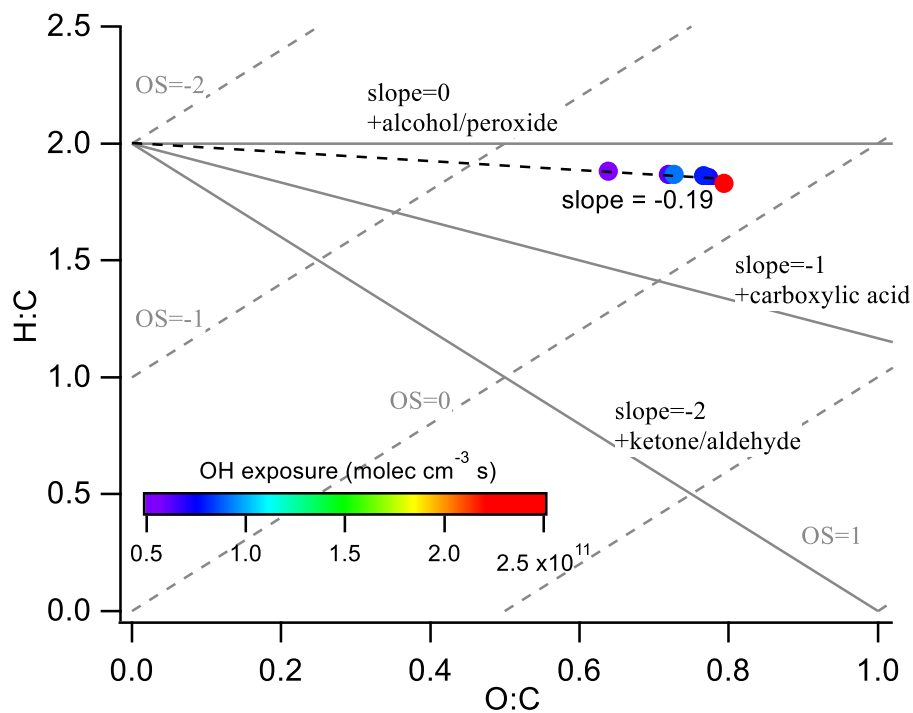
590 **Figure 2.** Highly complex mixture of canola oil SOA generated upon photooxidation. With known signal and mass fragmentation,  
591 signal of  $m/z$  73 can be recreated based on pseudo parent ions (e.g. M-15 used in this study).



592

593 **Figure 3.** Evolution in  $\overline{\text{OSc}}\text{-nc}$  space for canola oil SOA under different conditions of photochemical aging. As the oxidation  
 594 progresses in the atmosphere, more compounds are formed with smaller  $\text{nc}$  and higher  $\overline{\text{OSc}}$  suggesting fragmentation to be a  
 595 dominant pathway of oxidation for cooking emissions in the atmosphere.

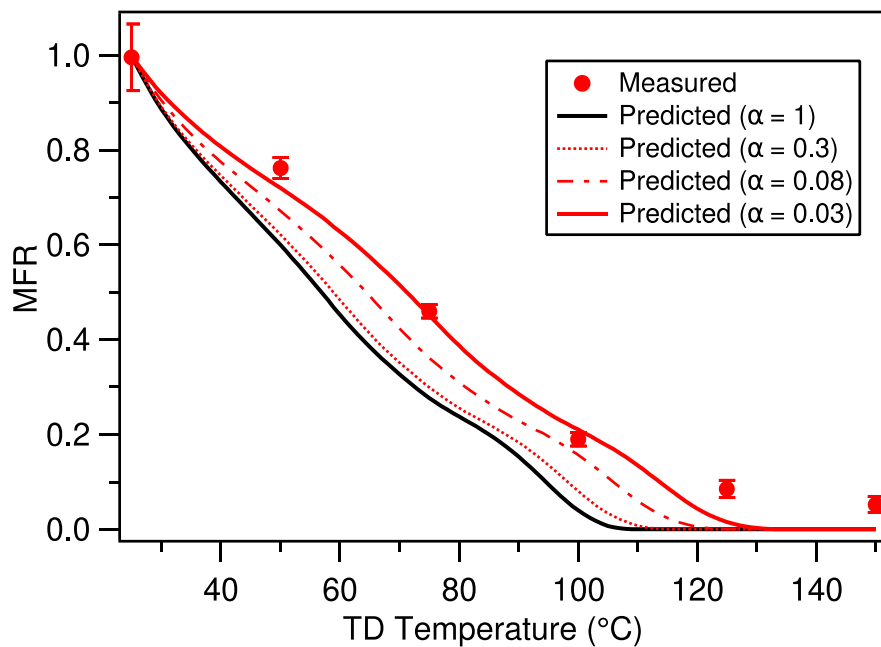
596



597

598 **Figure 4.** Van Krevelen diagram of canola oil SOA coloured by different OH exposure. In the background, average carbon  
 599 oxidation state ( $\overline{OS}_c$ ) and functionalization slopes are shown for reference. The slope of -0.19 for canola oil SOA corresponds to  
 600 formation of both alcohol and carboxylic acid consistent with the chemical composition obtained from TD-GC/MS.

601

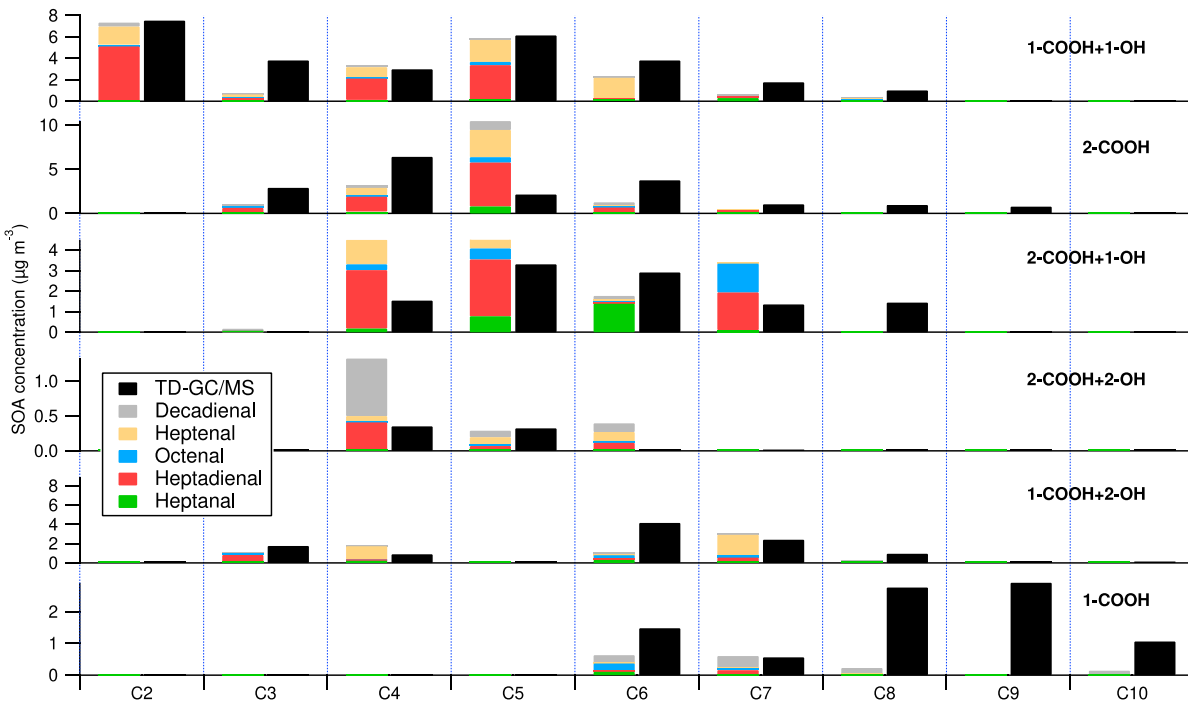


602

603 **Figure 5.** Mass thermogram of canola oil SOA at an OH exposure of  $9.23 \times 10^{10}$  molecules  $\text{cm}^{-3}$  s. The black line represents model  
 604 simulations using  $\alpha = 1$  underpredicting the measured MFR. The red line corresponds to model simulations using  $\alpha = 0.03$  predicting  
 605 the measurements reasonably well, therefore implying kinetic limitations in the system. The error bars represent  $\pm 1\sigma$ .

606

607

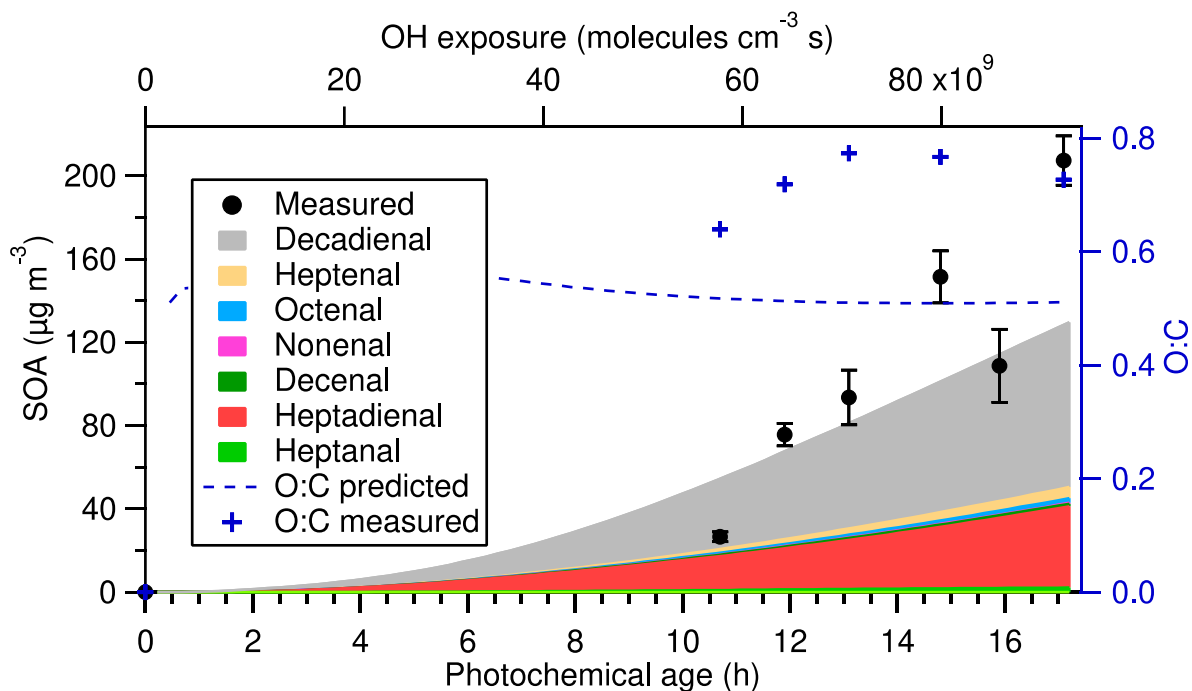


608

609 **Figure 6.** Prediction of different compounds formed at an OH exposure of  $6.43 \times 10^{10}$  molecules  $\text{cm}^{-3}$  s using product molar yields  
 610 of heptanal, heptenal, octenal, heptadienal, and decadienal. The total aldehydes products can explain the observed oil SOA products  
 611 within a factor of half, while the inconsistency in prediction of some SOA products is likely caused by differences in gas-particle  
 612 partitioning in both photooxidation systems.

613

614



615  
 616 **Figure 7.** SOM prediction of SOA produced from different aldehydes with increasing photochemical age. The model overpredicts  
 617 SOA formation at lower photochemical age, while underpredicts SOA formation by ~40% at higher photochemical age, suggesting  
 618 that traditional VOC precursors cannot fully explain the SOA formation, and other gas-phase precursors maybe needed to better  
 619 constrain the formation of SOA at higher aging conditions. In addition, the SOM predicted O:C is within 50% of the measured O:C  
 620 suggesting that the overall change in chemical composition of cooking SOA is predicted reasonably well.